

SUPPORTING INFORMATION

White Light Generation and Anisotropic Damage in Gold Films near Percolation Threshold

Sergey M. Novikov,[†] Christian Frydendahl,^{‡,§} Jonas Beermann,[†] Vladimir A. Zenin,[†] Nicolas Stengeri,^{‡,§} Victor Coello,^{||} N. Asger Mortensen,^{‡,§} and Sergey I. Bozhevolnyi^{,†}*

[†] Centre for Nano Optics, University of Southern Denmark, Campusvej 55, DK-5230 Odense, Denmark. [‡] Department of Photonics Engineering, Technical University of Denmark, DK-2800 Kongens Lyngby, Denmark. [§] Center for Nanostructured Graphene, Technical University of Denmark, DK-2800 Kongens Lyngby, Denmark. ^{||} CICESE Monterrey, Alianza Centro No.504 PIIT Apodaca, N. L. C. P. 66600, Mexico.

*Correspondence authors e-mail: seib@mci.sdu.dk

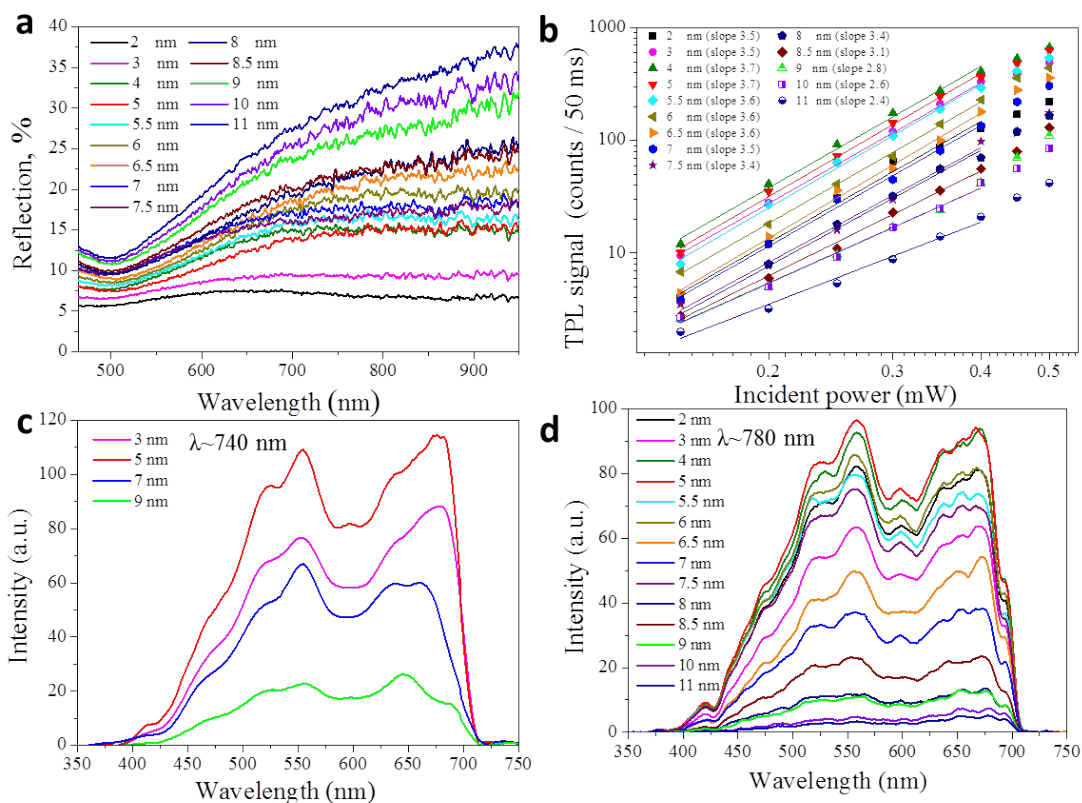


Figure S1. Characterization of thin gold films on glass substrate. **(a)** Reflection spectra obtained for the thin gold films and normalized as explained in Methods. **(b)** Dependence of TPL signal on the incident power. The data (points) were fitted with lines, whose slope indicates the order of TPL dependence on the power. The fitting was done until the power of 0.4 mW, because higher power might cause damage. Luminescence spectra obtained at the excitation wavelength of **(c)** 740 and **(d)** 780 nm. The arbitrary unit used in **(c)** and **(d)** corresponds to 10 counts/50 ms or 200 counts/s, respectively.

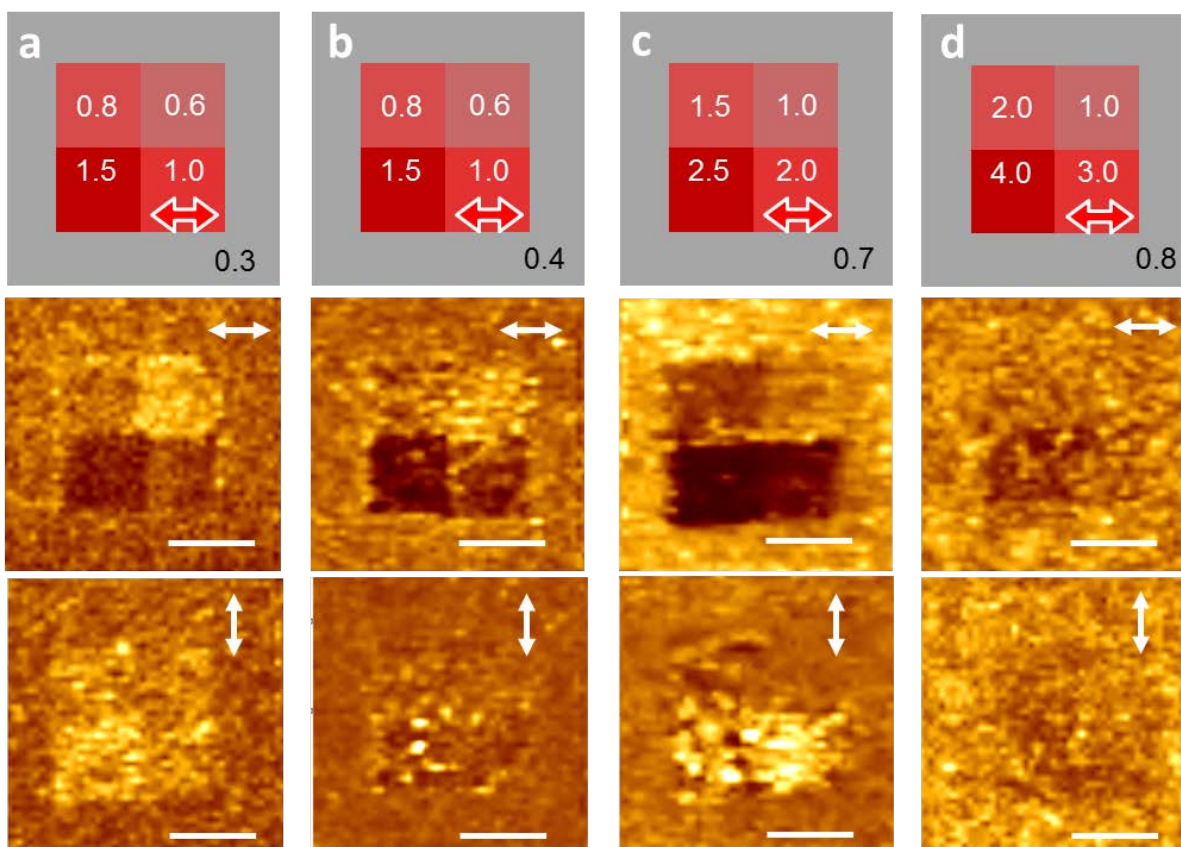


Figure S2. Polarization dependent TPL imaging. TPL images obtained for thin gold films on glass substrates with film thickness of (a) 3, (b) 5, (c) 7 and (d) 9 nm. Top: a schematic view of written squares (red) with numbers indicating used the writing laser power in mW. Numbers in the low right corner of grey square indicate the laser power in mW used for the read-out. Arrows indicate the electric field polarization direction of the scanning laser used for writing (top) and reading (central and bottom rows). The scale bars are 5 μm .

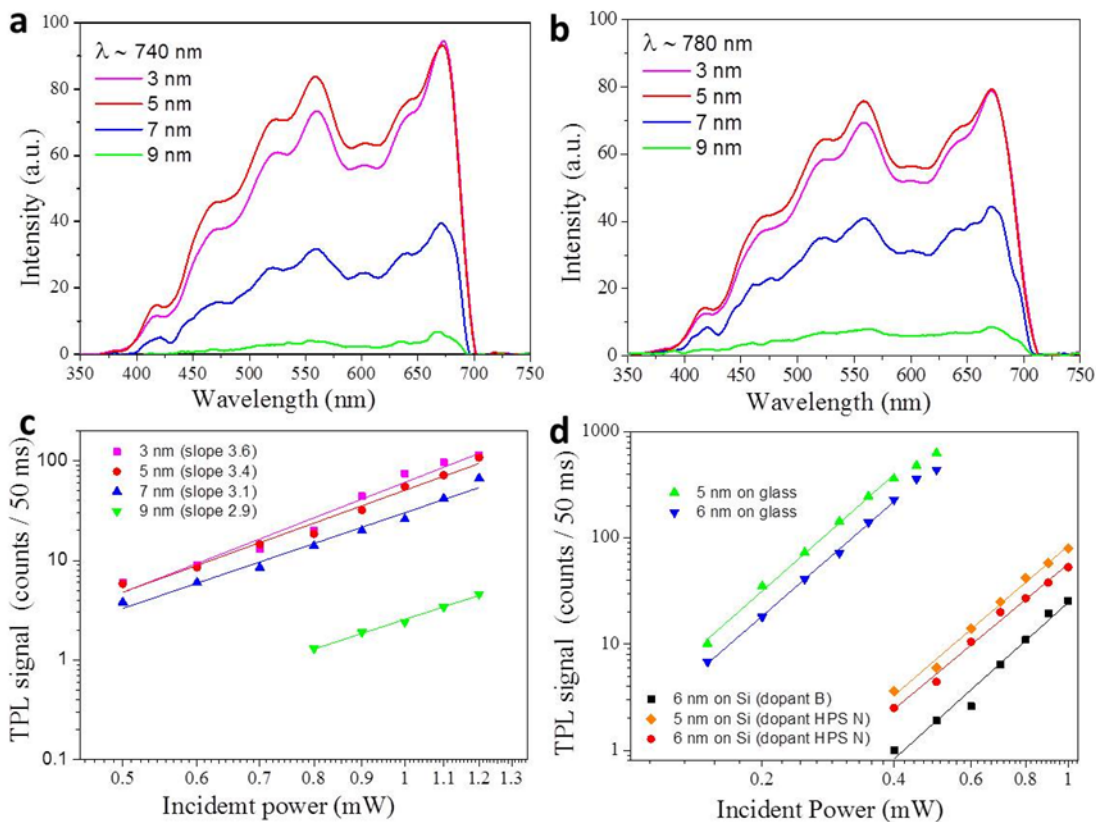


Figure S3. Substrate influence on the TPL. Luminescence spectra obtained for the excitation wavelength of (a) 740 and (b) 780 nm for thin gold films with thicknesses of 3 (magenta), 5 (red), 7 (blue) and 9 nm (green) on silicon substrates. (c) Dependences of TPL signals on the incident power for gold films on silicon substrates. The data (points) were fitted with lines, whose slope indicates the order of TPL dependence on the power. (d) TPL power dependences for the 5- and 6-nm-thin gold films deposited on glass and silicon (with different dopants) substrates. The arbitrary units used in (a) and (b) correspond to 10 counts/50 ms or 200 counts/s.

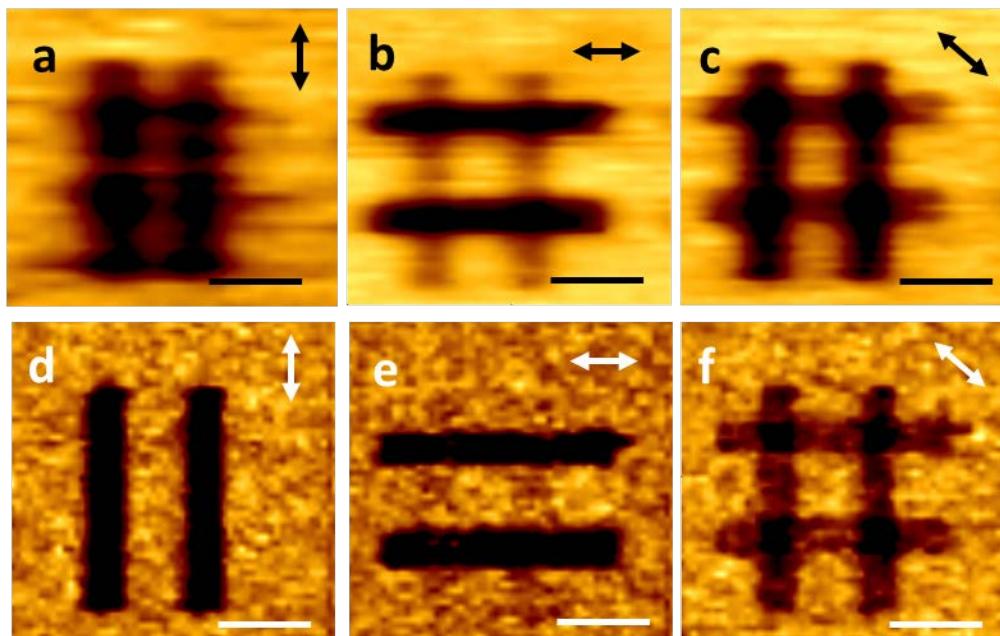


Figure S4. Comparing FH and TPL images during the read-out. (a)-(c) FH and (d)-(f) TPL images obtained from the 5-nm-thin gold film on a silicon substrate upon reading with the polarization direction indicated with a double arrow. Both writing and reading are carried out at the wavelength of 740 nm. The scale bars are 5 μm .

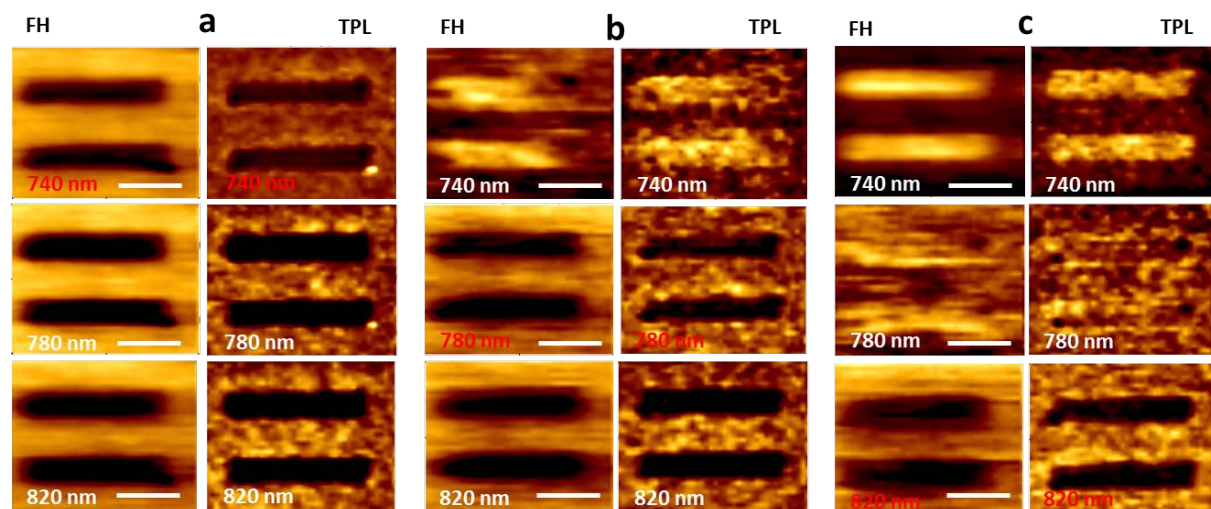


Figure S5. Wavelength dependent TPL imaging. The fundamental harmonic (left) and TPL (right) images obtained from the 5-nm-thin gold film on a silicon substrate. The writing was carried out at the wavelength of (a) 740, (b) 780, and (c) 820 nm. The FH wavelength used for reading was 740 nm (top row), 780 nm (middle row), and 820 nm (bottom row). Both writing and reading were conducted with the FH polarization direction along the written lines. The scale bars are 5 μm .

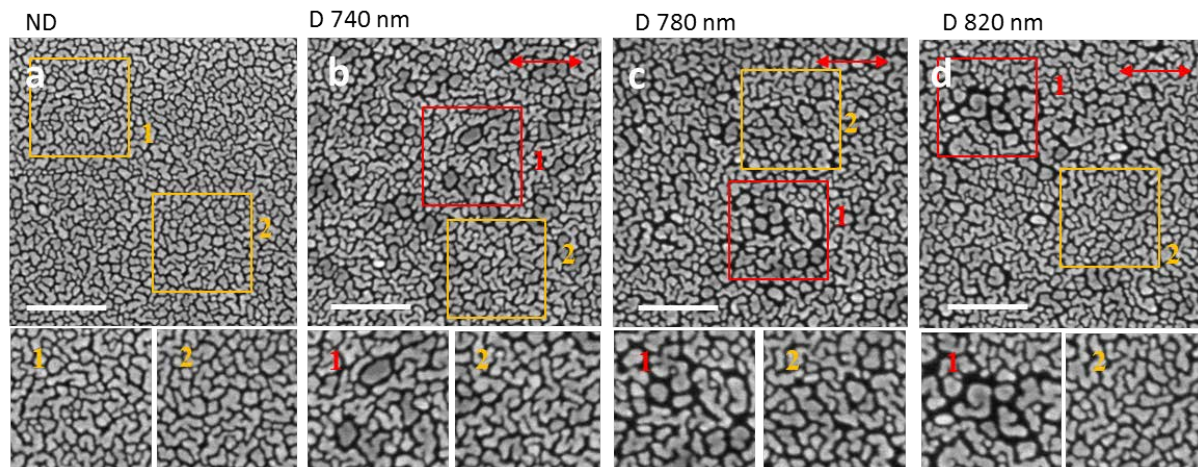


Figure S6. SEM characterization. SEM images obtained with the 5-nm-thin gold film on a silicon substrate (**a**) before and after damage inflicted at (**b**) 740, (**c**) 780, and (**d**) 820 nm. Orange frames indicate areas without noticeable damage while red frames show areas with melted clusters (bottom panels show enlarged frames). The scale bars are 250 nm.

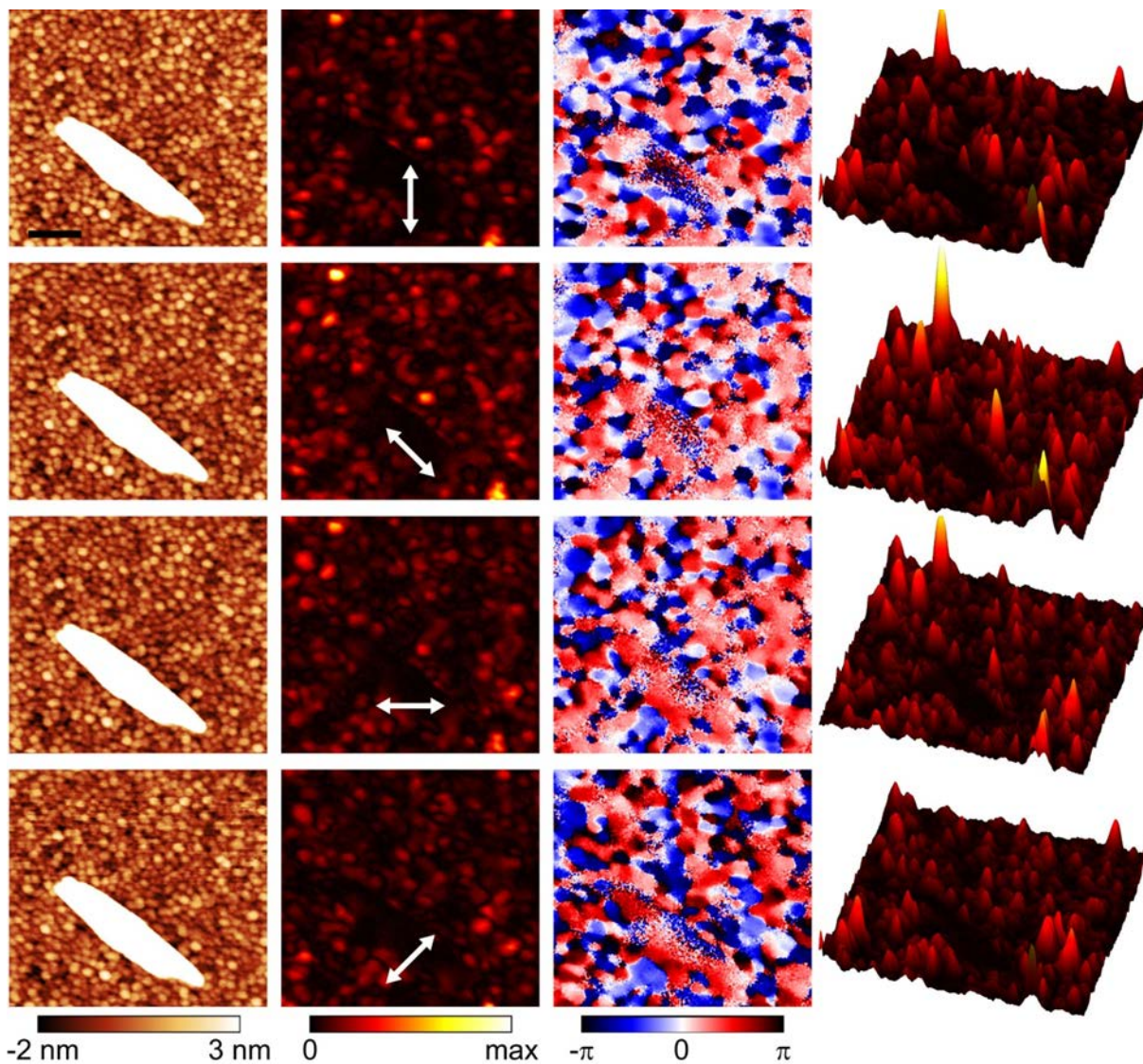


Figure S7. Polarization dependent SNOM images. Pseudocolour SNOM images of topography (left), optical near-field amplitude (middle) and phase (right) of the pristine 5-nm-thin gold film on a glass substrate. Right most column shows amplitude maps in 3D. Double arrows represent the illumination polarization of the telecom laser ($\lambda = 1500$ nm). White mark (visible in topography) was used for alignment. The scale bar is 200 nm.

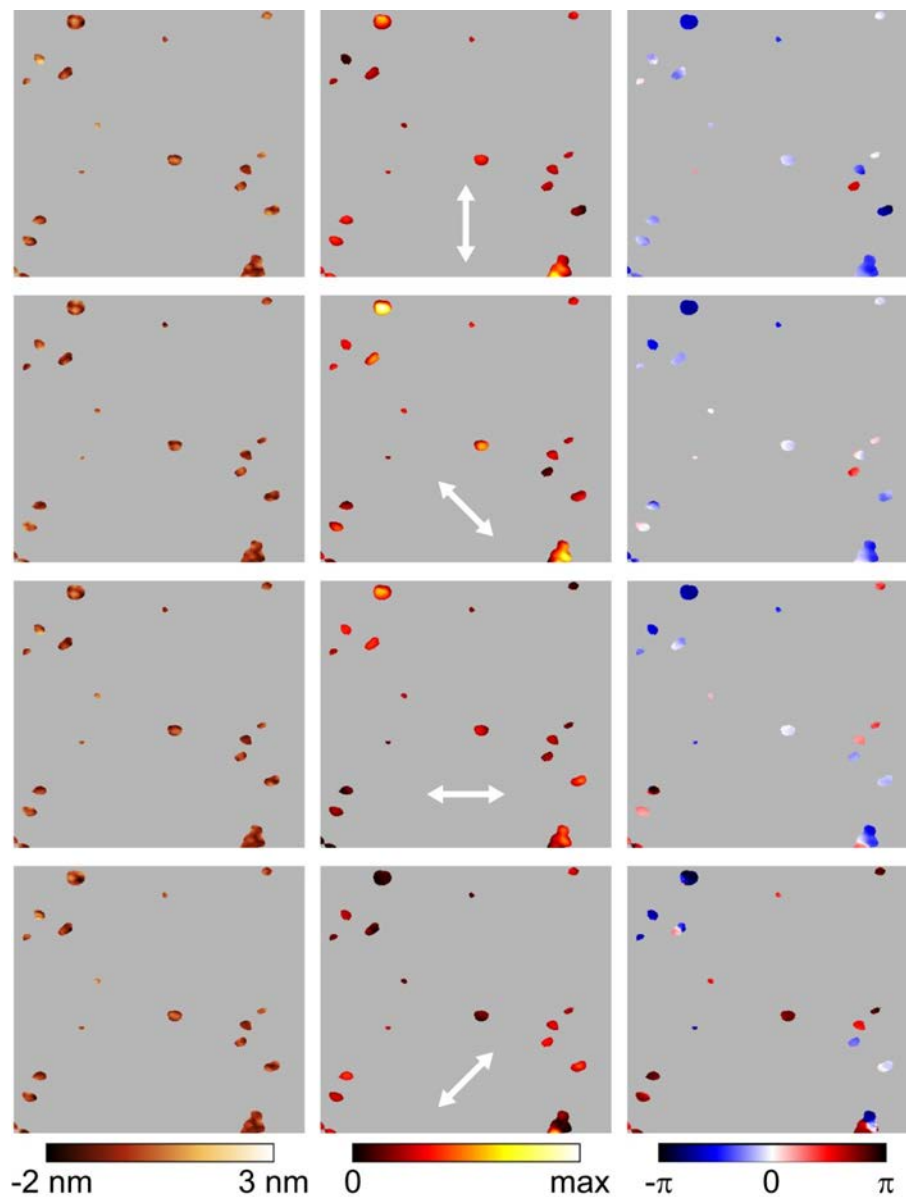


Figure S8. Identification of hot spots. The same as in Supplementary Fig. 7 SNOM images of topography (left), optical near-field amplitude (middle) and phase (right) of the pristine 5-nm-thin gold film on glass substrate, masked by the same mask. The mask was made from the average near-field amplitude (for all polarizations) to highlight hot spots. Double arrows represent the illumination polarization of the telecom laser ($\lambda = 1500$ nm).

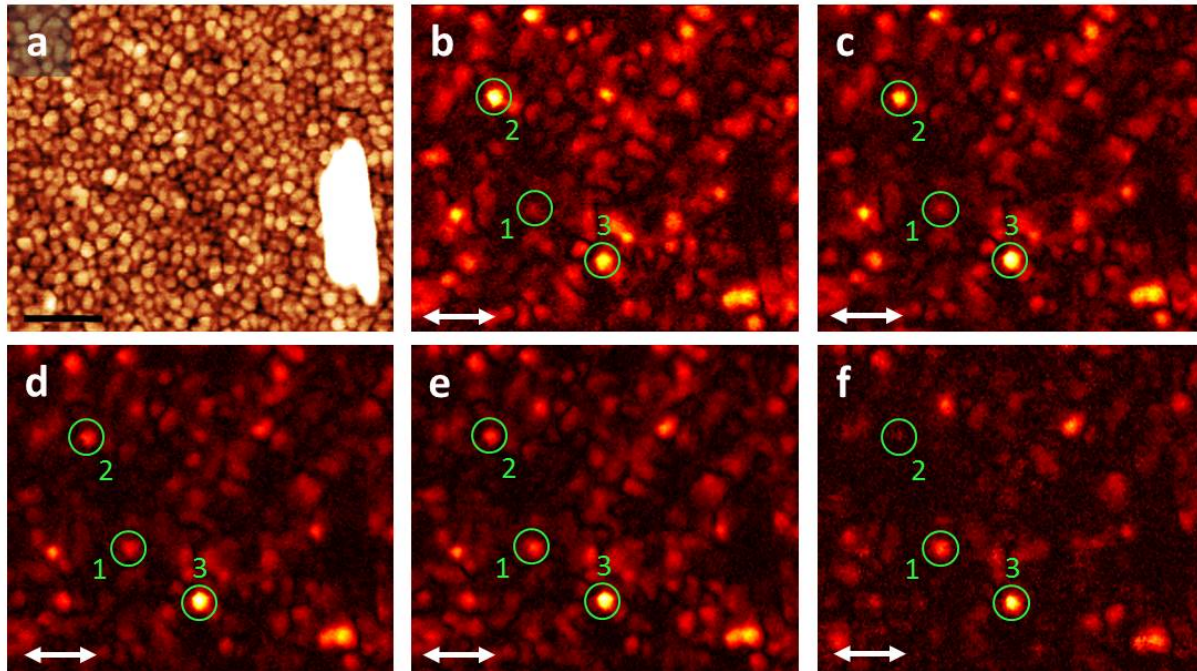


Figure S9. Wavelength dependent SNOM images. Pseudocolour SNOM images of (a) topography and (b)-(f) optical near-field amplitude of undamaged 5-nm-thin gold film on glass substrate at the illumination wavelength of (b) 1425, (c) 1475, (d) 1525, (e) 1575 and (f) 1625 nm, respectively. Double arrows represent the illumination polarization, kept constant for all wavelengths. White mark (visible in topography) was used for alignment. Colour maps are the same as in Supplementary Fig. 7. Each near-field amplitude image was normalized to the maximum at the given illumination wavelength. The scale bar is 200 nm. Green circles in (b)-(f) encircle the same hot spots.

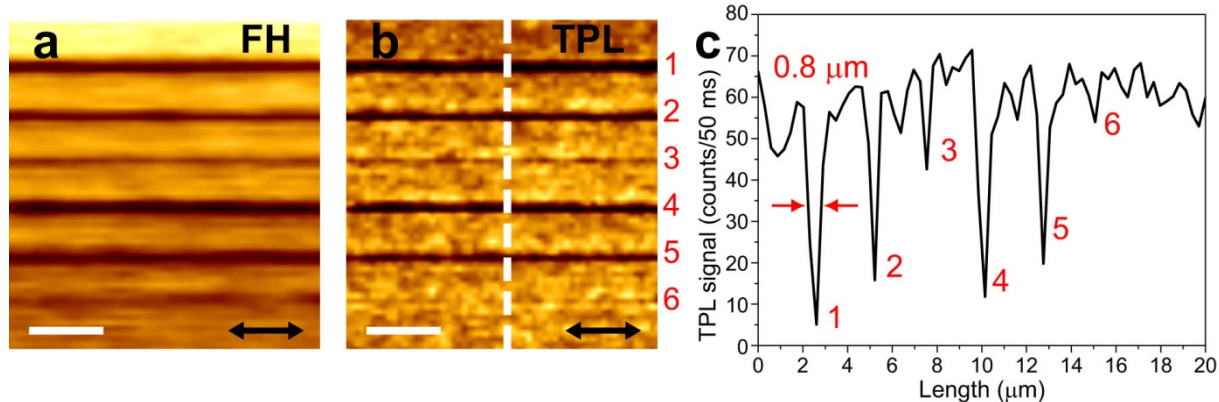


Figure S10. Estimation of the energy required for writing. **(a)** FH and **(b)** TPL images of the 5-nm-thin gold film on a silicon substrate, obtained with different FH powers during the writing procedure (with the exposure time of 50 ms and the scanning speed of 20 $\mu\text{m/s}$) and different scanning steps. For the scanning step of 360 nm, the FH writing powers are $P_1 \sim 5$ mW, $P_2 \sim 4$ mW, $P_3 \sim 3$ mW, whereas for the scanning step of 800 nm, $P_4 \sim 5$ mW, $P_5 \sim 4$ mW, $P_6 \sim 3$ mW. **(c)** Cross sections taken from the place marked by the dashed line in **(b)**. The scale bars are 5 μm .

Supplementary discussion

1. Estimation of the field enhancement

Let us consider the origin of two-photon luminescence (TPL) signals measured with both optically thick and very thin, island-like, gold films. We assume that the TPL signal is produced inside gold and leaves gold nanostructures without much absorption, since gold becomes increasingly transparent for wavelengths shorter than 600 nm.¹ TPL mechanism implies that the TPL power depends quadratically upon the incident light power or, alternatively expressed, upon the fourth power of the electric field magnitude, $|E_g|$, inside the gold:

$$P_{\text{TPL}} = \xi \int_V |E_g|^4 dV , \quad (1)$$

where ξ is a proportionality constant depending on gold properties and the illumination wavelength, and the integration is performed only inside the gold volume.

Considering the TPL signal from optically thick gold films (or bulk gold), we first express the electric field inside the gold using Fresnel relations and assuming normal incidence and relatively weak focusing:

$$E_g(x, y, z) = \frac{2}{n_g + 1} E(x, y) \exp\left[i \frac{2\pi}{\lambda} n_g z\right] , \quad (2)$$

where $E(x, y)$ is the incident electric field amplitude at the gold surface (z is the depth coordinate) and n_g is a complex-valued refractive index of gold: $n_g = 0.1686 + 4.5824i$ at the light wavelength $\lambda = 750$ nm.¹ The TPL power from the bulk gold can then be found using Eqs. (1) and (2) as follows:

$$\begin{aligned} P_{\text{TPL}}^b &= \frac{16}{(|n_g + 1|)^4} \xi \int_V |E(x, y)|^4 dx dy \left| \exp\left[i \frac{2\pi}{\lambda} n_g z\right] \right|^4 dz = \\ &= \left\| \begin{array}{l} n_{gi} = \text{Im}(n_g) \gg \text{Re}(n_g) \\ \delta_{\text{TPL}} = \lambda/8\pi n_{gi} \end{array} \right\| \cong \frac{16\xi}{n_{gi}^4} \delta_{\text{TPL}} \int_S |E(x, y)|^4 dx dy \end{aligned} , \quad (3)$$

with δ_{TPL} characterizing the TPL skin depth, which amounts to ~ 6.5 nm at $\lambda = 750$ nm. In evaluating the depth integral, we have implicitly assumed the film thickness to significantly exceed δ_{TPL} . Introducing the average magnitude E_{in} of the incident electric field and the incident beam spot area S , allows us to finally obtain:

$$P_{\text{TPL}}^b \cong \frac{16\xi}{n_{gi}^4} \delta_{\text{TPL}} E_{in}^4 S . \quad (4)$$

Considering the TPL signal from thin, island-like, gold films, we disregard depth variations (*i.e.*, along the z coordinate) of the incident electric field inside gold films to simplify the analysis (also the films are thinner than 10 nm). Our analysis of near-field images with the size similar to that of the incident laser beam in TPL experiments (see Figure 5 and Figure S8) indicates that the integration of the fourth power of the near-field amplitude over the whole image area and only over the brightest in the image spot (hot spot) produces the results different by ~ 5 times:

$$p \int_S |E_{\text{NF}}|^4 dx dy = \|p \cong 0.2\| = \int_{\text{hot spot}} |E_{\text{NF}}|^4 dx dy \cong E_{\text{max}}^4 S_{\text{hs}} , \quad (5)$$

where E_{max} is the maximum magnitude of the electric field (in the strongest hot spot) and $S_{\text{hs}} \cong (30 \text{ nm})^2$ is a typical size of the hot spot in near-field images. During the TPL imaging, the illuminating laser beam would occasionally miss the brightest hot spot available resulting in the variations of the detected TPL signal on the level of 10% (see Figure 2e), which is consistent with Eq. (5) deduced from the near-field images. We further note that the strongest electric field is expected to occur inside narrow gaps between gold islands (as is discussed in detail in the main text and corroborated with images in Figure 4). For gaps being much smaller than the free-space wavelength, the electric field inside the gap is oriented predominantly perpendicular to the gap boundaries and enhanced due to the boundary conditions.² The latter allows us to relate the strongest field in the gap, E_{max} , to the corresponding field inside the gold, $E_{g \text{ max}}$, that generates the TPL:

$$E_{\max} = \left| n_g^2 E_{g \max} \right| \Rightarrow E_{g \max} \cong \frac{E_{\max}}{n_{gi}^2} . \quad (6)$$

Assuming additionally that the relation expressed by Eq. (5) can also be applied to the field inside the gold, we can relate the TPL power measured with a film of thickness t to the maximum gap electric field:

$$P_{\text{TPL}}^f = \xi \int_V |E_g|^4 dV = \xi t \int_S |E_g|^4 dx dy = \xi t \frac{1}{p} E_{g \max}^4 S_{\text{hs}} = \frac{\xi t}{p} \left(\frac{E_{\max}}{n_{gi}^2} \right)^4 S_{\text{hs}} . \quad (7)$$

The obtained formulae, Eq. (4) and Eq. (7), allow us to estimate the electric field intensity enhancement, α , in the strongest hot spots of a given sample (with respect to the incident field intensity) by relating the TPL power measured with the sample and with an optically thick gold film (the reference sample) for the same illuminating beam:

$$\alpha = \frac{E_{\max}^2}{E_{in}^2} \cong 4n_{gi}^2 \sqrt{\frac{P_{\text{TPL}}^f}{P_{\text{TPL}}^b}} \sqrt{\frac{p \delta_{\text{TPL}} S}{t S_{\text{hs}}}} . \quad (8)$$

The first factor in the above formula comes from the difference in the relations between the fields inside and outside gold [cf. Eq. (2) and Eq. (6)]. The second factor takes into account the difference in the TPL signals measured, while the third one compares the effective volumes of gold from which TPL signals originate. Often the TPL measurements are conducted with incident laser beams of different powers that are adjusted individually so as to have sufficiently strong TPL signals without damaging illuminated regions. Introducing the powers of incident beams for the considered cases as P_{FH}^b and P_{FH}^f , respectively (“FH” stands for “fundamental harmonic” for historical reasons³), obtains the final expression:

$$\alpha = \frac{E_{\max}^2}{E_{in}^2} \cong 4n_{gi}^2 \sqrt{\frac{P_{\text{TPL}}^f}{P_{\text{TPL}}^b} \frac{P_{\text{FH}}^b}{P_{\text{FH}}^f}} \sqrt{\frac{p \delta_{\text{TPL}} S}{t S_{\text{hs}}}} . \quad (9)$$

Considering the TPL measurements conducted with a 5-nm-thin gold film on glass, the contribution from the first factor is ~ 85 , while the ratio of the TPL powers normalized to the same incident power is ~ 80 ($P_{\text{TPL}}^b \cong 7$ counts/50 ms $\cong 140$ counts/s at $P_{\text{FH}}^b = 10$ mW ,

$P_{\text{TPL}}^f \cong 10 \text{ counts}/50 \text{ ms} \cong 200 \text{ counts/s}$ at $P_{\text{FH}}^f = 0.15 \text{ mW}$). For the same 5-nm-thin gold film on glass, taking $p = 0.2$, $\delta_{\text{TPL}} \cong 6.5 \text{ nm}$, $S = (500 \text{ nm})^2$, $t = 5 \text{ nm}$, $S_{\text{hs}} \cong (30 \text{ nm})^2$, the third factor is ~ 8.5 . All in all, the intensity enhancement factor is estimated as $\alpha \sim 6 \cdot 10^4$.

Considering various assumptions involved in our estimation of the intensity enhancement [Eq. (9)], probably the most important one is related to the usage of the same proportionality constant, ξ , in both cases [cf. Eq. (1) and Eq. (7)]. This assumption disregards the influence of configuration geometry on the TPL process, which is essentially the process of photon emission with its rate being influenced by the local density of states (that can also be expressed by the Purcell factor). This implies that the TPL signal can strongly be enhanced by resonant characteristics of a gold nanostructure at the emission wavelength,^{4,5} whereas our consideration takes into account the field enhancement only at the wavelength of illumination [Eq. (5)]. It is clear that, since we attempt on isolating the intensity enhancement in the *brightest* hot spots, we should incorporate also this mechanism of TPL enhancement. While it is very challenging to theoretically describe this effect for irregular island-like films, one can make use of the available experimental results on the TPL enhancement caused by particle resonances at the TPL wavelength and estimate this TPL power enhancement as < 100 .^{4,5} Decreasing correspondingly the TPL power used in Eq. (9), results in the *final* (conservative) estimate of the field intensity enhancement: $\alpha \sim 6 \cdot 10^3$.

2. Comparison with other configurations

Let us compare the obtained estimate of the intensity enhancement, $\alpha \sim 6 \cdot 10^3$, with those reported in literature. White light generation and non-quadratic TPL power dependences were also observed for dimer gold antennas.⁶ For this configuration, the authors calculated the maximum field intensity enhancement in the plane located 10 nm above gold antennas as ~ 200 for the gap of 30 nm. Without going into details of their estimation procedure, we note that the gap width influences the size of a hot spot, and, in our case, is expected to be *considerably* smaller, at least for the films that are near the percolation threshold. In a very recent work devoted to radiation nanofocusing by using tapered metal stripes terminated with impedance-matched resonant antennas,⁷ the estimated intensity enhancement of $\sim 12 \cdot 10^3$ was found inside a

10-nm-wide gap (with a square cross-section of $30 \times 30 \text{ nm}^2$). Even though this number is close to our estimate, we should note that these configurations are very different because, in the referred work,⁷ the average electric field inside the gap was compared to the average electric field of the propagating (along a metal stripe) plasmonic mode. A better number for comparison can be found in accompanying Figure S8, where the characteristics of a resonant dimer antenna with the same gap are displayed, indicating the intensity enhancement of $\sim 9 \cdot 10^3$.⁷ Even larger intensity enhancements, reaching $\sim 11 \cdot 10^3$, were reported when studying silver dimers consisting of 36-nm-diameter spheres with a 2-nm-wide gap, while the intensity enhancement of $\sim 5 \cdot 10^4$ was estimated for the same gap of 2 nm between two 12-nm-thin silver triangles having a side length of 60 nm in a bow-tie configuration.⁸ Note that, in this work, the estimations were conducted using the classical electrodynamics with a local response. Theoretical calculations based on a more accurate approach involving a nonlocal response predict the enhancement of $\sim 10^4$ inside a 1-nm-wide gap between two silver cylinders with radii of 15 nm.⁹ Therefore, our estimate of the intensity enhancement, $\alpha \sim 6 \cdot 10^3$, seems to be a reasonable value, also because, for very thin, island-like gold films near the percolation threshold all different gap widths are expected.

Supplementary References

- (1) Palik, E. D. *Handbook of optical constants of solids*. 1985, Academic Press: Orlando.
- (2) Søndergaard, T. and Bozhevolnyi, S. Slow-plasmon resonant nanostructures: Scattering and field enhancements. *Phys. Rev. B*. **2007**, 75, 073402.
- (3) Beermann, J.; Evlyukhin, A.; Boltasseva, A. and Bozhevolnyi, S. I. Nonlinear microscopy of localized field enhancements in fractal shaped periodic metal nanostructures. *J. Opt. Soc. Am. B*. **2008**, 25, 1585-1592.
- (4) Lumdee, C., Yun, B. and Kik, P. G. Gap-plasmon enhanced gold nanoparticle photoluminescence. *ACS Photonics*. **2014**, 1, 1224–1230.
- (5) Andersen, S. K. H.; Pors, A. and Bozhevolnyi, S. I. Gold photoluminescence wavelength and polarization engineering. *ACS Photonics*. **2015**, 2, 432–438.
- (6) Mühlischlegel, P., Eisler, H. J., Martin, O. J. F., Hecht, B. & Pohl, D. W. Resonant optical antennas. *Science*. **2005**, 308, 1607–1609.

- (7) Zenin, V. A.; Andryieuski, A.; Malureanu, R.; Radko, I. P.; Volkov, V. S.; Gramotnev, D. K.; Lavrinenko, A. V. and Bozhevolnyi, S. I. Boosting local field enhancement by on-chip nanofocusing and impedance-matched plasmonic antennas. *Nano Lett.* **2015**, *15*, 8148-8154.
- (8) Hao, E. and Schatz, G. C. Electromagnetic fields around silver nanoparticles and dimers. *J. Chem. Phys.* **2004**, *120*, 357–366.
- (9) Raza, S.; Bozhevolnyi, S. I.; Wubs, M. and Mortensen, N. A. Nonlocal optical response in metallic nanostructures. *J. Phys.: Condens. Matter.* **2015**, *27*, 183204.